

## SURFACE BRIGHTNESS FLUCTUATIONS IN THE HUBBLE SPACE TELESCOPE ACS/WFC F814W BANDPASS AND AN UPDATE ON GALAXY DISTANCES\*

JOHN P. BLAKESLEE<sup>1,2</sup>, MICHELE CANTIELLO<sup>3</sup>, SIMONA MEI<sup>4,5</sup>, PATRICK CÔTÉ<sup>1</sup>, REGINA BARBER DEGRAAFF<sup>2</sup>,  
LAURA FERRARESE<sup>1</sup>, ANDRÉS JORDÁN<sup>6</sup>, ERIC W. PENG<sup>7</sup>, JOHN L. TONRY<sup>8</sup>, GUY WORTHEY<sup>2</sup>

*Accepted for publication in ApJ*

### ABSTRACT

We measure surface brightness fluctuation (SBF) magnitudes in the F814W filter and ( $g_{475}-I_{814}$ ) colors for nine bright early-type Fornax cluster galaxies imaged with the *Hubble Space Telescope* Advanced Camera for Surveys (ACS). The goal is to achieve the first systematic SBF calibration for the ACS/F814W bandpass. Because of its much higher throughput, F814W is more efficient for SBF studies of distant galaxies than the ACS/F850LP bandpass that has been used to study nearby systems. Over the color range spanned by the sample galaxies,  $1.06 < (g_{475}-I_{814}) < 1.32$  (AB mag), the dependence of SBF magnitude  $\bar{m}_{814}$  on ( $g_{475}-I_{814}$ ) is linear to a good approximation, with slope  $\sim 2$ . When the F850LP SBF distance measurements from the ACS Fornax Cluster Survey are used to derive absolute  $\bar{M}_{814}$  magnitudes, the dependence on ( $g_{475}-I_{814}$ ) becomes extremely tight, with a slope of  $1.8 \pm 0.2$  and scatter of 0.03 mag. The small observed scatter indicates both that the estimated random errors are correct, and that the intrinsic deviations from the SBF-color relation are strongly correlated between the F814W and F850LP bandpasses, as expected. The agreement with predictions from stellar population models is good, both in slope and zero point, indicating that our mean Fornax distance of 20 Mpc is accurate. The models predict curvature in the relation beyond the color limits of our sample; thus, the linear calibration should not be extrapolated naively. In the Appendices, we reconsider the Tonry ground-based and Jensen NICMOS SBF distance catalogues; we provide a correction formula to ameliorate the small apparent bias in the former, and the offset needed to make the latter consistent with other SBF studies. We also tabulate two new SBF distances to galaxies observed in the ACS Virgo Cluster Survey.

*Subject headings:* galaxies: distances and redshifts — galaxies: clusters: individual (Fornax) — galaxies: elliptical and lenticular, cD

### 1. INTRODUCTION

The measurement of galaxy distances has been a central problem in astronomy ever since the discovery of “spiral nebulae” by Lord Rosse in the mid-nineteenth century. Because geometric methods were of no avail, the nature of these objects remained a matter of conjecture for many decades. Only with the work of Henrietta Swan Leavitt did accurate photometric distance estimates to resolved stellar systems become a reality. Her painstaking photographic measurements of the light curves for 1800 variable stars (and hundreds of comparison stars) in the Magellanic Clouds led her to note that for variables of a certain class, the brighter ones had longer temporal periods (Leavitt 1908). The Leavitt Law, relating the luminosities of Cepheid variables to their periods, proved to be the key to the mystery of the spiral nebulae, locating them firmly beyond the spatial extent of our own Galaxy; thus it was also the key to comprehending the true scale of

the Universe, eventually accomplished with the work of Hubble (1926, 1929).

Accurate galaxy distances remain of fundamental importance to most astrophysical applications. Errors in distance estimates generally translate into equal or larger fractional uncertainties in derived quantities such as masses (of everything from central black holes to dark matter haloes), linear sizes, dynamical timescales, star formation rates, and ages. Thus, accurate distance estimation is essential for inter-comparing the physical properties of galaxies in the local volume where redshift is not a reliable indicator of distance, and for comparing the properties of nearby galaxies to those at high redshift. Of course, they are also essential for mapping local three-dimensional structures and velocity fields.

There are a variety of distance indicators that can be used within and beyond the limit of classical Cepheid distances; Freedman & Madore (2010) provide a recent overview of the methods. One of the most accurate of these is surface brightness fluctuations (SBF; Tonry & Schneider 1988; for a historical review, see Blakeslee et al. 2009, hereafter ACSFCS-V). The SBF method measures the intrinsic variance in a galaxy image resulting from the random variations in the numbers and luminosities of the stars falling within individual pixels of the image. This variance is normalized by the local galaxy surface brightness and then converted to the apparent SBF magnitude  $\bar{m}$ . The distance modulus,  $\bar{m}-\bar{M}$  follows once the absolute magnitude  $\bar{M}$  is known.

The value of  $\bar{M}$  in a given bandpass depends on the stellar population properties. For early-type systems, a single broad-baseline color generally suffices for characterizing the stellar population (e.g., Tonry et al. 1997; Ajhar et al. 1997; Fer-

\* Based on observations with the NASA/ESA *Hubble Space Telescope*, obtained from the Space Telescope Science Institute, which is operated by AURA, Inc., under NASA contract NAS 5-26555.

<sup>1</sup> Herzberg Institute of Astrophysics, National Research Council of Canada, Victoria, BC V9E 2E7, Canada; John.Blakeslee@nrc.ca

<sup>2</sup> Department of Physics and Astronomy, Washington State University, Pullman, WA 99163-2814

<sup>3</sup> INAF-Osservatorio Astronomico di Teramo, via M. Maggini, I-64100, Teramo, Italy

<sup>4</sup> University of Paris Denis Diderot, 75205 Paris Cedex 13, France

<sup>5</sup> GEPI, Observatoire de Paris, Section de Meudon, 5 Place J. Janssen, 92195 Meudon Cedex, France

<sup>6</sup> Departamento de Astronomía y Astrofísica, Pontificia Universidad Católica de Chile, Santiago 22, Chile

<sup>7</sup> Department of Astronomy, Peking University, Beijing 100871, China

<sup>8</sup> Institute for Astronomy, University of Hawaii, Honolulu, HI 96822

rarese et al. 2000; Blakeslee et al. 2001; Mei et al. 2005b; ACSFCS-V). The zero-point of the  $I$ -band  $\overline{M}$  calibration has been tied directly to the Cepheid distance scale to an accuracy of 0.08 mag, or  $\sim 4\%$  in distance, from ground-based SBF measurements in spiral bulges (Tonry et al. 2000). For distance estimation purposes, SBF is best measured in the reddest optical bandpasses. The fluctuations arise mainly from red giant branch stars and thus are brighter at redder wavelengths. However, the stellar population dependence becomes more complicated in the near-infrared (Jensen et al. 2003), which adds intrinsic scatter to that application of the method. Thus, the red end of the optical spectrum is something of a “sweet spot” for SBF.

The SBF method has been an important part of two recent *Hubble Space Telescope* (*HST*) surveys of early-type cluster galaxies carried out with the Advanced Camera for Surveys’ Wide Field Channel (ACS/WFC). The 100-orbit ACS Virgo Cluster Survey (ACSVCS; Côté et al. 2004) and the 43-orbit ACS Fornax Cluster Survey (ACSFCS; Jordán et al. 2007) both observed one galaxy per orbit, with the time split between the F475W and F850LP filters. The SBF analysis was performed on the F850LP ( $z_{850}$ -band) images, while the second bandpass enabled the calibration of the SBF  $z_{850}$  magnitude in terms of  $(g_{475}-z_{850})$  color (Mei et al. 2005b; ACSFCS-V). These single-orbit observations were adequate at the distances of the Virgo and Fornax clusters, but for galaxies significantly farther away, the relatively low throughput of F850LP can make the required exposure times prohibitive. The F814W filter then becomes more attractive for SBF work simply because the higher total throughput of this passband reduces the exposure time by at least a factor of two. However, although there have been some ACS/WFC measurements of SBF in this bandpass (Cantiello et al. 2007a,b; Barber DeGraaff et al. 2007; Biscardi et al. 2008), there has been no systematic empirical calibration of the SBF method in F814W similar to that in F850LP. The main goal of the present work is to provide such a calibration that will be applicable to the bright early-type galaxies targeted at large distances.

The following section presents our observational sample and basic imaging reductions. Section 3 describes our SBF and color measurements in detail and compares the results to our previous F850LP measurements. Section 4 provides a comparison with predictions from stellar population models and discusses the uncertainty in the absolute distance to the Fornax cluster. Section 5 presents the conclusions from this study. In Appendix A, we revisit the ground-based SBF distances from Tonry et al. (2001) and provide a simple correction formula for possible bias in those distances. Finally, Appendix B presents two additional SBF distance measurements from the ACSVCS F475W and F850LP imaging data.

## 2. OBSERVATIONS AND IMAGE REDUCTIONS

The proximity ( $\sim 20$  Mpc) and compactness of the elliptical-rich Fornax cluster makes it the ideal target for calibrating the stellar population dependence of the SBF method in any bandpass (e.g., Tonry 1991; ACSFCS-V). As we are mainly interested in the calibration for luminous early-type galaxies, we selected the eight brightest Fornax galaxies as listed by Jordán et al. (2007), all of which have  $M_B < -19$ . Because of the precision of ACS/WFC SBF measurements, this sample was deemed suitable for deriving a calibration accurate to about  $\pm 0.02$  mag over the normal color range for giant ellipticals.

As part of *HST* program GO-10911, we observed six fields

with the ACS/WFC targeting large galaxies in the Fornax cluster. Each observation consisted of three dithered exposures in the F814W filter totaling 1224 s and two dithered exposures in F475W totaling 680 s. The galaxy NGC 1375 is separated by only  $2'.4$  from its neighbor NGC 1374, and we were able to fit them both along the  $4'.7$  diagonal of a single ACS/WFC field of view. NGC 1374 was placed in the upper left quadrant of the field, on the same CCD chip on which the other giant galaxies were centered, while NGC 1375 was simultaneously in the lower right quadrant. Although NGC 1375 is 1.4 mag fainter than the limit of the other eight, it provides extra leverage for constraining the calibration slope and was available gratis. In addition, we downloaded suitable F814W data from the *HST* archive on the Fornax galaxies NGC 1316 (from GO-9409, PI: Goudfrooij) and NGC 1344 (from GO-9399, PI: Carter) and suitable F475W data on the same two galaxies from GO-10217 (PI: Jordán). Table 1 summarizes the properties and basic observational details for our nine target galaxies, including the  $z_{850}$  SBF distances from the ACSFCS-V.

The exposures were bias and dark current subtracted and flatfielded by the standard STScI pipeline processing. The calibrated “fit” data were then run through the Apsis pipeline (Blakeslee et al. 2003) to produce geometrically rectified, clean, combined images. Apsis uses Drizzle (Fruchter & Hook 2002) for the geometric transformation of the images, and we use the Lanczos3 interpolation kernel in order to preserve the essential properties of the image power spectra (see Mei et al. 2005a). All photometry reported here is on the AB system, calibrated based on Sirianni et al. (2005) and Bohlin (2007) with the revised zero points from the ACS instrument website<sup>10</sup> for data obtained before July 2006. In particular, we adopted:  $m_1(\text{F475W}) = 26.0809$ ,  $m_1(\text{F814W}) = 25.9593$ , where  $m = -2.5 \log(f) + m_1$ , and  $f$  is in electrons per second. The ACS/WFC F814W and F475W bandpasses closely approximate the Kron-Cousins  $I$  and Sloan Digital Sky Survey  $g$  bands, so we refer to magnitudes in these bandpasses as  $g_{475}$  and  $I_{814}$ , respectively. We corrected for Galactic extinction using the dust maps from Schlegel et al. (1998) with the extinction ratios given by Sirianni et al. (2005). The extinction in this direction is small,  $E(B-V) \lesssim 0.02$  mag.

## 3. SBF ANALYSIS

### 3.1. Measurements within Annuli

There have been a variety of implementations of the SBF analysis within different reduction packages (e.g., Tonry et al. 1990; Lorenz et al. 1993; Pahre et al. 1999; Nielsen & Tsvetanov 2000; Liu et al. 2002; Mieske et al. 2003; Mei et al. 2005a; Cantiello et al. 2005; Dunn & Jerjen 2006), but few detailed comparisons between them. One notable exception is the comparison made by Pahre et al. (1999) of their SBF results for one galaxy observed with *HST*/WFPC2 with the results for the same observation using the Tonry et al. (1990, 1997) software. They found good agreement for this one case. Otherwise, the comparisons have mainly been between sets of published numbers, rather than tests of different analysis procedures applied to the same data.

In order to ensure that our calibration is as general as possible, we performed two complete sets of SBF reductions on all the galaxies. We first used the custom SBF analysis software developed by J. Tonry within the Vista environment<sup>11</sup> for

<sup>10</sup> <http://www.stsci.edu/hst/acs/analysis/zeropoints>

<sup>11</sup> <http://www.ifa.hawaii.edu/~jt/soft.html>

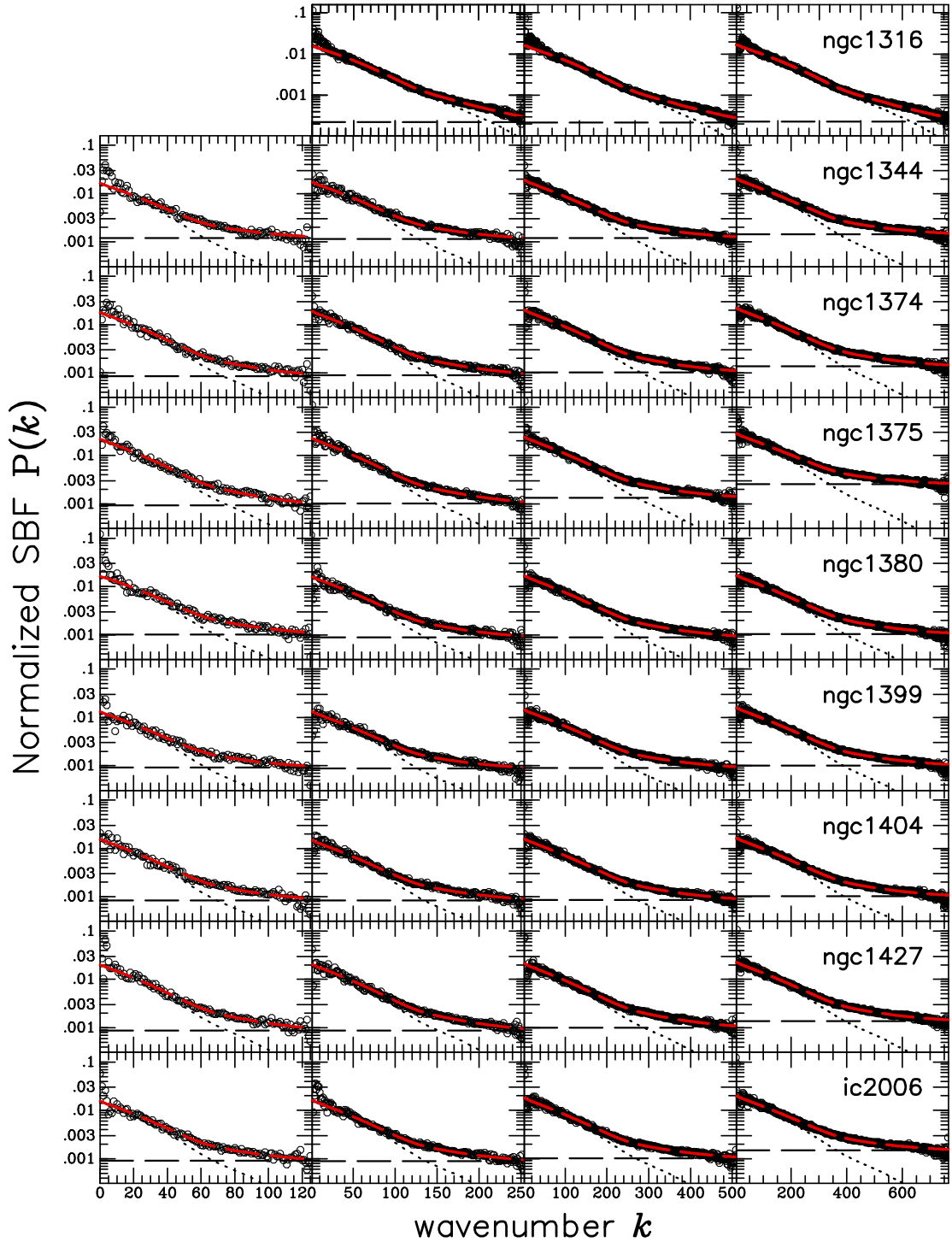


FIG. 1.— Power spectrum measurements for different annuli within our program galaxies (labeled); the radii of the annuli increase from left to right, as described in the text. The red curves show our fits to the power spectra. Because of the significant dust features, the annuli for NGC 1316 differ from the other galaxies', and only three were used. The power spectra are normalized by the local galaxy surface brightness, so that the amplitude  $P_0$  of the PSF component (dotted curve) corresponds to the SBF magnitude  $\bar{m}$ , after a small  $\lesssim 2\%$  correction for background variance.

the ground-based SBF survey (Tonry et al. 1997) and applied most recently to *HST*/ACS data by Barber DeGraaff et al. (2007). We refer to this set of reductions as the ‘‘Tonry’’ SBF analysis; details can be found in the referenced works and several others that have used the same software (e.g., Blakeslee et al. 1997; Jensen et al. 1998). These reductions tend to be interactive, with the user selecting radial limits for the analysis regions within each galaxy and power spectrum fitting limits. Second, we applied the identical SBF analysis code as used in ACSFCS-V, which was only slightly modified from the analysis routines developed and used by Mei et al. (2005a,b). These routines are written in IDL and the SBF analysis is more automated, which facilitates multiple runs to test for systematics effects. As an example, Mei et al. (2005a) reran the analysis numerous times on simulated images processed with Apsis to assess the effects of different Drizzle interpolation kernels.

While there are no fundamental differences between the two analysis codes likely to cause any significant disagreements, the current data set affords a useful test of the level consistency that can be expected. For both sets of SBF measurements, we model and subtract the galaxy, mask all visible sources, and estimate the residual variance from undetected sources as detailed in our previous works (Mei et al. 2005b; Barber DeGraaff et al. 2007; Jordán et al. 2004, 2007; ACSFCS-V). These steps are the same for nearly all implementations of the SBF method, and we used the same galaxy models and background variance corrections for both sets of reductions. For this sample of high-resolution, high-throughput F814W ACS imaging data, the estimated background corrections ranged from 0.011 to 0.019 mag. As in our previous works, we assign 25% uncertainty to these values, meaning that the contribution to the total error in the SBF magnitude is less than 0.005 mag. This contrasts strongly with ground-based analyses, for which the source detection limits tend to be much brighter and the background variance correction is often a major source of uncertainty. We masked dusty regions in the galaxy images as described in Ferrarese et al. (2006) by taking the ratio of the images in the two bands and identifying areas that significantly deviated from the smooth color profile. The dust masks were augmented by hand as needed. The two galaxies in our sample with significant dust features are NGC 1316 and NGC 1380. Thus, this comparison of SBF analyses does not address possible problems with galaxy modeling or residuals due to dust or other contaminants. However, the consistency of the results as a function of radius within a galaxy can be used to check for such problems.

Both the Tonry and IDL analysis procedures are performed in a series of annuli with increasing radii. The inner radius of the innermost annulus was  $6''.4$  (128 pix) for all galaxies except the dusty post-merger galaxy NGC 1316, for which it was  $12''.8$ . The outer radius of each annulus was typically twice its inner radius, although for the IDL code we used a maximum annular width of 256 pix to be more similar to our past analyses, and only annuli where the galaxy  $I_{814}$  surface brightness is at least twice the sky background were used. For the Tonry code analysis, we set the maximum outer radius somewhat arbitrarily at 1000 pix, except in the case of the faintest galaxy NGC 1375, for which it was 512 pix. The two different analysis procedures independently calculate the power spectra and fit the amplitude of the component that has been convolved with the point spread function (PSF), which corresponds to the SBF signal after correcting for the background variance. Section 3.2 discusses systematic effects from different PSFs.

In fitting the power spectra, the IDL code omits the lowest wavenumbers, those representing spatial scales larger than 20 pix, since these are affected by the galaxy and large-scale background light subtraction, and it also omits the several highest wavenumbers because of the pixel correlation introduced by the geometric correction (see Mei et al. 2005 for details). However, with the adopted Lanczos3 kernel, the pixel correlation is very mild and the power spectrum fit is not very sensitive to the maximum wavenumber, assuming that the PSF model is accurate. The Tonry code also omits the lowest numbers, although this is done interactively by selecting the point where the fitted amplitude  $P_0$  of the PSF component becomes stable. There is no option in this code to omit the highest wavenumbers, so this is another difference in the analyses. Figure 1 displays power spectra fits for multiple annuli within the program galaxies from the IDL analysis code. The signal is very strong and well fitted in all cases; note the logarithmic scale.

The two analysis procedures both measure the  $(g_{475}-I_{814})$  color in each annulus after applying the same mask as used for the SBF measurement. We then calculate the biweight means of the color and SBF measurements from among the annuli to get the average values for each galaxy. We note that radial color gradients are common in early-type galaxies and SBF magnitudes follow the same trends. SBF and color gradients have been studied in ACS imaging data from a stellar population perspective by Cantiello et al. (2005, 2007a). All of the galaxies in our sample have detectable color gradients except the bluest galaxy NGC 1375. However, as found by ACSFCS-V, the presence of such gradients is not a problem for our averaging procedure as long as the SBF–color relation is approximately linear over the color range within each galaxy. Figure 2 shows SBF and color measurements for the individual annuli within the galaxies. The top panel plots the observed values of  $\bar{m}_{814}$ , while the lower panel plots absolute  $\bar{M}_{814}$  after subtracting the  $z_{850}$  SBF distance moduli from ACSFCS-V. There is a clear trend between SBF magnitude and  $(g_{475}-I_{814})$  color, well approximated by a linear relation. The scatter is about  $\sim 30\%$  lower for  $\bar{M}_{814}$  as compared to  $\bar{m}_{814}$ . The improvement in scatter for a quadratic fit, as compared to linear one, is not significant.

The mean difference in galaxy SBF magnitudes from the Tonry and IDL power spectrum analyses was  $0.005 \pm 0.005$  mag, with an rms scatter of 0.017 mag, which is within the range of the measurement errors. Only NGC 1316 showed an absolute difference as large as 0.03 mag because of the difficulty in selecting ‘‘clean’’ regions in this dusty galaxy; for the other eight, the difference was 0.02 mag or less. This represents the first detailed comparison between the two analysis codes that have been used most extensively for SBF measurement. The close agreement gives us confidence that our SBF calibration is applicable to either one. Here we adopt the results from the IDL analysis simply because it is the same code as used in our past ACS/WFC studies, and the steps have been described in detail by those works. Table 2 presents the final SBF and color measurements, as well as the distance information derived from the calibration presented below.

### 3.2. Effect of the Point Spread Function

As noted in the previous section, the SBF measurement involves fitting the amplitude of the component of the power spectrum that has been convolved with the PSF of the image. Thus, the PSF template is an important consideration

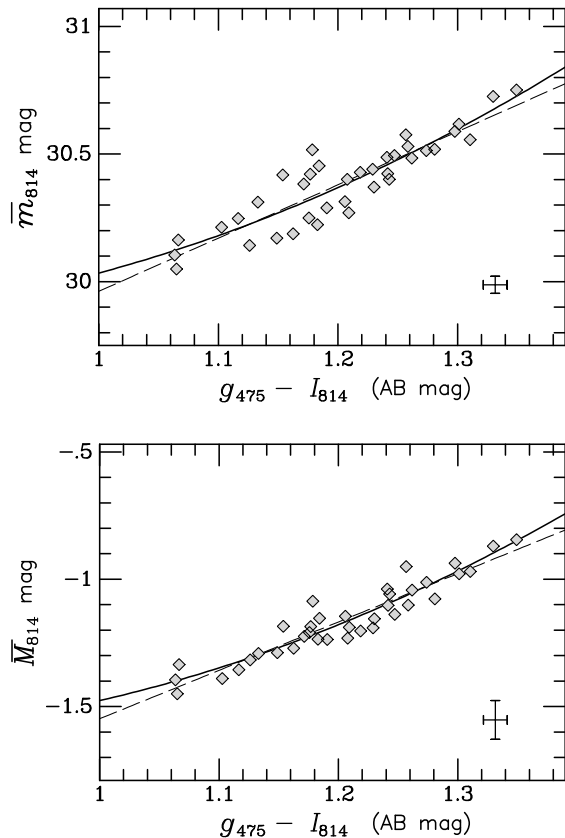


FIG. 2.— *Top*: apparent SBF magnitude as a function of  $(g_{475}-I_{814})$  color for individual annuli within the nine program galaxies. *Bottom*: mean absolute SBF magnitudes after subtracting the individual distance moduli from ACSFCS-V are plotted versus color. The dashed lines are simple linear least-squares fits, while the solid curves show quadratic fits for comparison. Representative measurement errors are indicated in the lower right of each panel; the  $\bar{M}_{814}$  error bar includes the typical distance uncertainty.

in the analysis. The ACSVCS and ACSFCS analyses (Mei et al. 2005b; ACSFCS-V) both used a composite empirical PSF constructed from archival images by Blakeslee et al. (2006) for deconvolving the profiles of high-redshift cluster galaxies. The PSF variation within ACS/WFC images after distortion-corrected is small (Krist 2003) and occurs on small scales (largest wavenumbers) that do not significantly affect the power spectrum fits (Mei et al. 2005a), although a 2% error in the fitting for different annuli was assumed in ACSFCS-V (as well as here, since the same code was used) from the spatial variation in the PSF. However, tests by Mei et al. (2005a) and Cantiello et al. (2005, 2007b) using multiple ACS/WFC PSF stars (generally taken from different images) found variations of 0.02–0.05 mag in the final  $\bar{m}_{814}$  values. Similar, though slightly larger, variations of 0.04–0.06 mag were found in tests using multiple PSFs in ground-based data with a variable PSF and in *HST*/NICMOS data (Blakeslee 1999; Jensen et al. 2001). The variations in  $\bar{m}$  are due to a combination of effects, including errors in determining the correct normalization of each PSF template (systematic for a given data set), and mismatch between the PSF template and galaxy image (potentially random, if the PSF varies from image to image).

For this study, we searched all of our fields for relatively isolated stars that were bright but unsaturated, and could be used to make a high signal-to-noise model of the PSF power spectrum. The density of stars in these fields, which are at

Galactic latitude  $b \approx -54^\circ$ , is low. We found only one suitable star, which was in the IC 2006 field, and used this as our primary PSF template. We also tried PSFs from other data sets and reran the full IDL power spectrum analysis to assess the effect on  $\bar{m}_{814}$ . The ACS Instrument Development Team made available the composite PSFs constructed from the white dwarf spectrophotometric standard stars analyzed by Sirianni et al. (2005) and processed with the same interpolation kernel. The composite star for the F814W bandpass has been used for some previous SBF studies (Barber DeGraff et al. 2007; Cantiello et al. 2005, 2007a,b). When we used this template, our final  $\bar{m}_{814}$  values became systematically fainter by 0.036 mag. We also tried individual stars from a random ACS F814W image that we had available, and the final  $\bar{m}_{814}$  values became brighter by a similar amount.

Consistent with previous studies, these tests indicate variations of  $\sim 0.04$  mag from the PSF. At least for the current, fairly homogeneous, data set, any error of this size resulting from the PSF must be mainly systematic, affecting all the results in the same way, since the scatter in the calibration presented below is less than this, and is consistent with known measurement errors. The low density of Galactic foreground stars makes it difficult to characterize the PSFs in the individual images, but no significant image-to-image variations were found in the mean full widths at half maximum. The fact that we are using a high signal-to-noise template from one of our program fields should ensure that the PSF is accurate for that field, and by extension, given the small scatter that we find for the final calibration (and the quality of the power spectrum fits), the PSF template appears accurate for the full sample. However, it may be beneficial for future SBF studies that use our calibration to compare the results that they obtain with the PSF used here (available from the authors).

### 3.3. SBF Calibration for F814W

Figure 3 plots the SBF magnitudes versus  $(g_{475}-I_{814})$  color for our sample of nine Fornax galaxies, similar to Figure 2, but here using the final averaged quantities for each galaxy. Fitting a linear relation for  $\bar{m}_{814}$  in terms of  $(g_{475}-I_{814})$ , including errors in both axes and an additional 0.06 mag of intrinsic (or “cosmic”) scatter in  $\bar{m}_{814}$  at fixed  $(g_{475}-I_{814})$  due to stellar population effects (ACSFCS-V), we find

$$\bar{m}_{814} = (30.384 \pm 0.024) + (2.10 \pm 0.33)[(g_{475}-I_{814}) - 1.2], \quad (1)$$

where  $(g_{475}-I_{814}) = 1.2$  mag is the mean color of our sample. The quoted error bars reflect the fit uncertainties. The rms scatter is 0.064 mag, consistent with measurement errors plus the expected intrinsic scatter and small depth within Fornax (ACSFCS-V).

We could shift this calibration by the mean distance modulus of  $31.54 \pm 0.02$  mag for our nine sample galaxies, but since we have good  $z_{850}$  SBF measurements for each one, and want the calibrations of the two bandpasses to be as consistent as possible, we instead derive absolute  $\bar{M}_{814}$  magnitudes using the individual distance measurements. The lower panel of Figure 3 shows the results, which give the following calibration fit:

$$\bar{M}_{814} = (-1.168 \pm 0.013 \pm 0.092) + (1.83 \pm 0.20)[(g_{475}-I_{814}) - 1.2], \quad (2)$$

which is valid for AB colors  $1.06 < (g_{475}-I_{814}) < 1.32$  mag. The rms scatter of the data points with respect to this linear

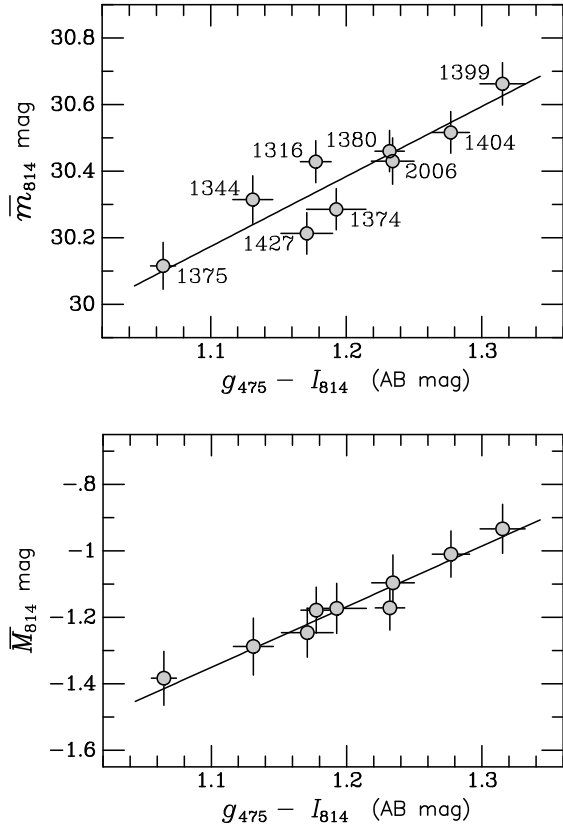


FIG. 3.— The F814W SBF calibration. *Top*: mean apparent SBF magnitude as a function of  $(g_{475}-I_{814})$  color for the sample galaxies. The vertical error bars are the quadrature sums of the measurement errors and an intrinsic stellar population scatter of 0.06 mag, as estimated in ACSFCS-V. Horizontal error bars represent measurement errors. Galaxies are labeled by their catalogue numbers. *Bottom*: the mean absolute SBF magnitudes after subtracting the individual distance moduli from ACSFCS-V are plotted against color. The vertical error bars are the quadrature sums of the measurement errors and the distance error (which includes the intrinsic component) from ACSFCS-V. Horizontal error bars again represent measurement errors. The lines show linear fits including errors in both coordinates; the coefficients are given in Equations (1) and (2), respectively.

calibration is 0.029 mag, and the fit has been derived using the  $(g_{475}-I_{814})$  and  $\overline{m}_{814}$  measurement errors, plus 0.015 mag of additional error added in quadrature to make  $\chi_n^2 = 1.0$  and ensure that the fit errors are reasonable. It might seem more correct to include the errors in the individual distances used in determining the  $\overline{M}_{814}$  values. However, when we do this, we find  $\chi_n^2 = 0.2$ , which has less than a 2% probability of occurrence. The likely explanation relates to the behavior of the intrinsic scatter of 0.06 mag that was estimated by ACSFCS-V and has been included in the distance errors. This is the largest component of the error for some galaxies, and apparently it is strongly coupled between the F814W and F850LP bandpasses, so that  $\overline{M}_{814}$  and  $\overline{M}_{850}$  scatter in the same way (see the following section for more discussion). We have therefore omitted this part of the error in deriving the above fit, and add only 0.015 mag to make  $\chi_n^2$  unity. This 0.015 mag represents an allowance for differential intrinsic scatter between the two bands, although it may include a small contribution from some additional measurement error.

The first error bar on the constant coefficient in Equation (2) reflects the uncertainty from the fit, which is smaller than for

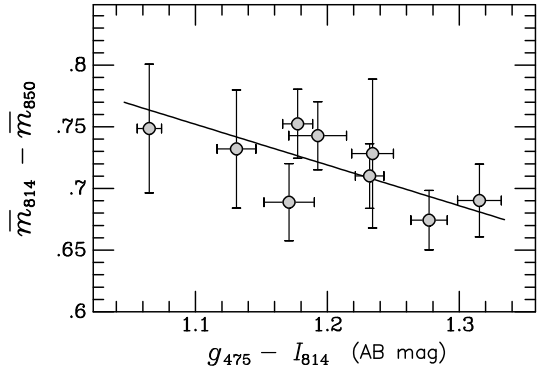


FIG. 4.— SBF color  $(\overline{m}_{814}-\overline{m}_{850})$  versus integrated color  $(g_{475}-I_{814})$  for the sample galaxies. There is some indication that this SBF color becomes slightly bluer as the galaxies get redder, but the slope of the plotted linear fit is significant at only the  $\lesssim 2\sigma$  level.

Equation (1) because the scatter of the data points is lower when using  $\overline{M}_{814}$ . The second error bar gives our estimate of the systematic uncertainty including the 0.08 mag for the tie of the SBF method to the Cepheid scale (Tonry et al. 2000, 2001; Ferrarese et al. 2000), 0.02 mag for the mean distance of these galaxies from ACSFCS-V, and 0.04 mag for the possible systematic error in the PSF normalization (Sec. 3.2). It does not include the additional uncertainty in the Cepheid distance scale, which may be of order  $\sim 0.1$  mag (Freedman & Madore 2010).

Table 2 lists the SBF distance moduli  $(m-M)_{814}$  and linear distances  $d_{814}$  derived for the current sample using the calibration given by Equation (2). The tabulated distance uncertainties reflect the total random errors, including measurement errors and the estimated 0.06 mag of intrinsic scatter. They do not include the systematic error in the calibration zero-point, which is common to all.

### 3.4. Comparison with $z_{850}$ -band SBF

It is useful to compare directly our  $I_{814}$  SBF magnitudes and distance estimates with the  $z_{850}$  results from ACSFCS-V. We find a mean “SBF color” for these galaxies of  $\overline{m}_{814}-\overline{m}_{850} = 0.72$ , with an rms of 0.027 mag. However, the SBF color decreases slightly, or gets “bluer,” as the SBF magnitudes get fainter in redder galaxies, as shown in Figure 4, where the fitted relation including errors in both coordinates is given by

$$\overline{m}_{814}-\overline{m}_{850} = (0.72 \pm 0.01) - (0.33 \pm 0.18)[(g_{475}-I_{814})-1.2], \quad (3)$$

with an rms scatter of 0.021 mag. The significance of the slope is slightly less than  $2\sigma$ , but the same trend occurs as a function of  $(g_{475}-z_{850})$ , with the same scatter. It is not too unusual for the SBF color to become bluer while photometric color becomes redder over some range in population parameters, especially when age is increased at fixed metallicity (Blakeslee et al. 2001). However, SBF and color measurements would be needed for more galaxies in more bandpasses to place strong constraints on the underlying populations. Put another way, the slope of  $\overline{m}_{814}$  as a function of  $\overline{m}_{850}$  is slightly less than one, as shown in the left panel of Figure 5, where the plotted linear fit has slope  $0.91 \pm 0.06$ . The rms scatter about this fit is 0.022 mag, which is consistent with random measurement errors, as the reduced  $\chi_n^2 = 0.8$  is reasonable for a linear fit to 9 data points. This supports our conclusion above that any intrinsic deviations in  $\overline{m}_{814}$  and  $\overline{m}_{850}$  due to stellar population effects must track closely between the two bands.

The right panel of Figure 5 provides a comparison of the

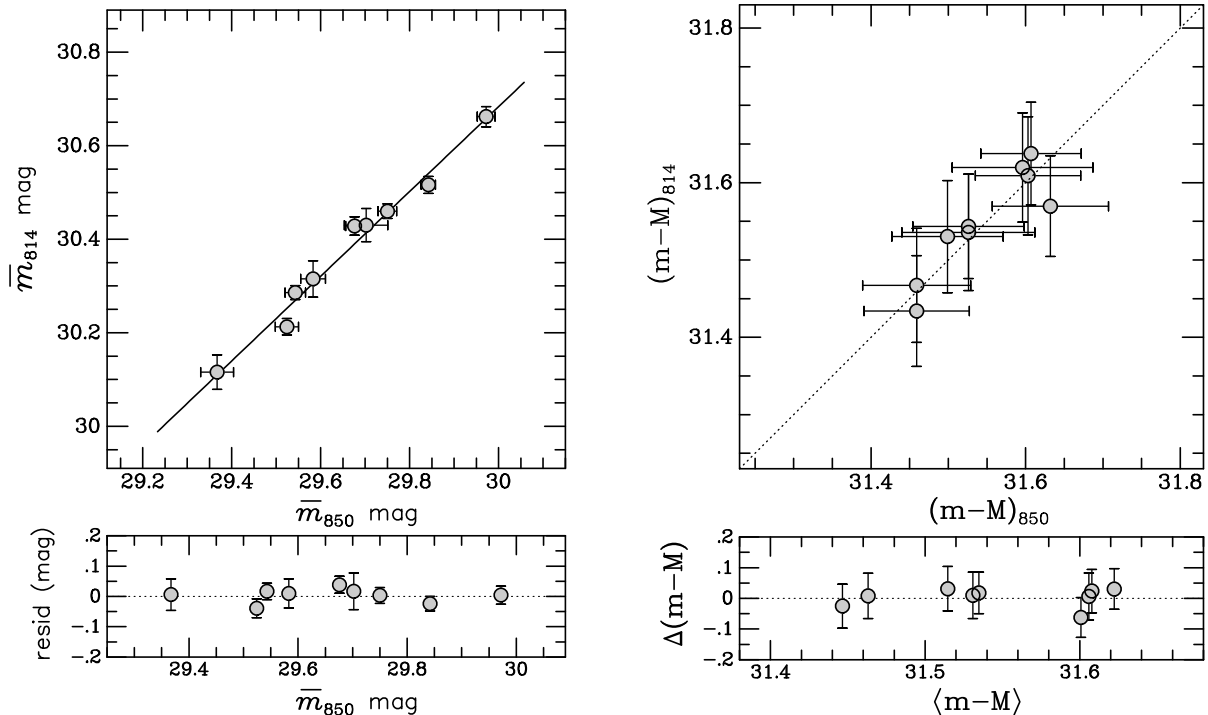


FIG. 5.— *Left*: SBF  $\bar{m}_{814}$  magnitude from this study is plotted against  $\bar{m}_{850}$  from ACSFCS-V. The errors bars include only measurement error. The slope of the linear fit is  $0.91 \pm 0.06$ , and the residuals are shown at bottom, with the error bars here being the quadrature sums of the measurement errors. *Right*: Distance modulus  $(m-M)_{814} \equiv (\bar{m}_{814} - \bar{M}_{814})$  from the current study using the calibration in Equation (2) is plotted against distance modulus  $(m-M)_{850} \equiv (\bar{m}_{850} - \bar{M}_{850})$  from ACSFCS-V. The dotted line shows equality, and the differences between the distance moduli are shown as a function of their average at bottom. The intrinsic component of the errors appears to be strongly correlated between the two bands; see text.

distance moduli from the present work using Equation (2) with those from ACSFCS-V. The plotted line indicates unity, and the mean difference between the two sets of measurements is zero by design, since the distance moduli from ACSFCS-V went into deriving the  $\bar{M}_{814}$  magnitudes used for the  $I_{814}$  calibration. The plotted error bars include the 0.06 mag of intrinsic scatter for each band, and naively using these errors,  $\chi_n \approx 0.1$ , which has only a  $\sim 0.2\%$  probability of occurring. Clearly, the intrinsic scatters in the SBF magnitudes in these two bandpasses are strongly correlated, and the two sets of measurements cannot be considered completely independent, even though they come from different data sets in different filters. However, this comparison is useful in that it shows the random measurement errors are small as expected,  $\lesssim 0.03$  mag. Further, the tight correlation ensures consistency of the ACSFCS-V distances with those measured here, and thus with future F814W SBF studies that use our calibration.

#### 4. MODEL COMPARISON AND THE DISTANCE TO FORNAX

The SBF distance zero point used in this study is an empirical one, ultimately tied to the metallicity-corrected Cepheid distance scale. More specifically, it assumes a mean distance of 16.5 Mpc to the Virgo cluster based on the Tonry et al. (2001) ground-based SBF distances recalibrated with the final set of *HST* Key Project Cepheid distances of Freedman et al. (2001); see Mei et al. (2005b) and Appendix A of the present work for further details. The mean distance of 20 Mpc for the Fornax cluster then comes from the measured  $0.42 \pm 0.03$  magnitude offset between the Virgo and Fornax (ACSFCS-V).

There is also a long history of attempts to calibrate the SBF method from stellar population modeling, thereby making it another “primary” distance indicator not tied to the Cepheids

(e.g., Worthey 1993; Buzzoni 1993; Blakeslee et al. 2001; Mei et al. 2001; Cantiello et al. 2003; Raimondo et al. 2005; Marin-Franch & Aparicio 2006). Biscardi et al. (2008) used the Teramo “SPoT” models<sup>12</sup> (Raimondo et al. 2005) in order to derive a theoretical linear calibration of the absolute SBF magnitude in the ACS/WFC F814W bandpass as a function of  $(g_{475} - I_{814})$  color. This is the same combination of bandpasses as we have calibrated here from an empirical standpoint, although we work in the AB system while Biscardi used the VEGAMAG system. The slope is of course unaffected by this difference, and their quoted value of  $2.2 \pm 0.2$  is close to our empirical results in Equations (1) and (2).

Comparisons between empirical calibrations and those derived from simple stellar population models are complicated because one is never sure which models best represents actual galaxies. But it is a useful exercise to check for general consistency. Figure 6 provides a direct comparison of our SBF and color observations with the predictions from the SPoT models, as in Biscardi et al. (2008) but transformed to the AB system. The top panel shows the loci for models with metallicities  $[\text{Fe}/\text{H}] = -0.7, -0.3, 0.0, +0.3$ , and ages ranging from 3 to 14 Gyr for each. We also show our measurements from Figure 3, along with the fit from Equation (2). The lower panel is similar, but symbols are used to show the model values for 6 different ages at each metallicity. The linear empirical calibration overlaps remarkably well with the locus of the solar metallicity models, which must be at least partly fortuitous, but consistent with the mean metallicities in these galaxies being not too far from solar. The curve in the lower panel is a cubic polynomial fit to the plotted models.

Two things are particularly worthy of note in Figure 6. First,

<sup>12</sup> <http://www.oao-teramo.inaf.it/SPoT>

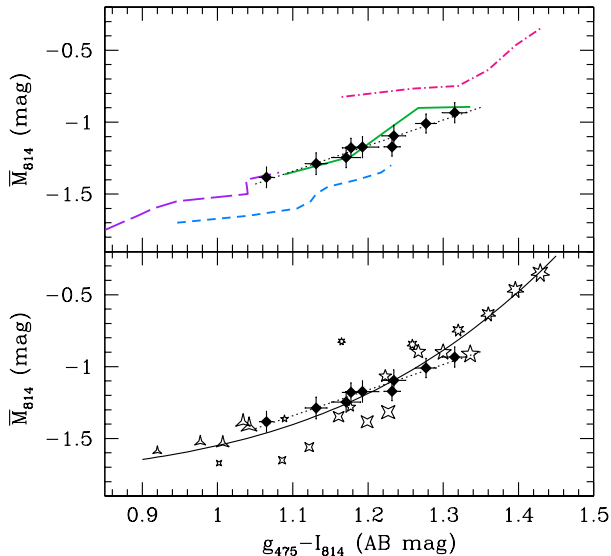


FIG. 6.— Comparison of SBF observations with model predictions. *Top*: interpolated curves for Teramo SPoT models with metallicities  $[\text{Fe}/\text{H}] = -0.7, -0.3, 0.0, +0.3$  (long-dashed purple, short-dashed blue, solid green, and dot-dashed red curves, respectively) and ages ranging from 3 to 14 Gyr. The age along each curve generally increases from left to right with photometric color. The predictions for the solar metallicity models (green solid curve) lie near the data points (black diamonds); the dotted line shows the empirical calibration. *Bottom*: similar to the top panel, but here the models with different  $[\text{Fe}/\text{H}]$  are represented by symbols having three ( $-0.7$ ), four ( $-0.3$ ), five (solar), and seven ( $+0.3$ ) points. Symbol size increases with age, and we plot model ages of 3, 5, 7, 9, 11, and 13 Gyr. The curve shows a cubic polynomial fit to the plotted models. Over the range of the observations, the fitted model relation follows the empirical one fairly well, but the models predict more curvature beyond this range, similar to what has been observed for  $\bar{m}_{850}$  over a larger range of galaxy colors.

there is remarkable consistency between the zero points of the observations and models. In fact, the fits to data and models cross very near the mean color of  $(g_{475} - I_{814}) = 1.2$ . The excellent agreement between two very different avenues for calibrating the F814W SBF magnitudes suggests that neither is likely to be far wrong, and thus the mean Fornax distance of  $\sim 20$  Mpc appears correct. Second, the fit to the model predictions indicates some curvature in the relation, similar to what we found in ACSFCS-V for the  $\bar{m}_{850}$  magnitudes of a larger sample of galaxies including dwarfs that extended to much bluer colors. Over the color range of the galaxies in our sample, the deviation between the linear and cubic fits is small, so the linear calibration suffices. However, one should not blindly apply this calibration beyond the fitted range, as it is reasonable to expect that the curvature may be significant.

## 5. SUMMARY

We have measured SBF  $\bar{m}_{814}$  magnitudes and  $(g_{475} - I_{814})$  colors for nine bright early-type galaxies in the Fornax cluster from new and archival *HST* ACS/WFC imaging data. We employed two different analysis procedures for measuring the SBF and found excellent agreement between them. For this sample of galaxies, which spans the color range  $1.06 < (g_{475} - I_{814}) < 1.32$  (AB mag), there is a clear trend of  $\bar{m}_{814}$

with  $(g_{475} - I_{814})$  that is well approximated by a linear relation of slope  $\sim 2$ . We have used the  $z_{850}$  SBF distances from ACSFCS-V to obtain absolute  $\bar{M}_{814}$  for all the galaxies and derive an empirical calibration of the  $I_{814}$  SBF method that is consistent with the large sample of existing  $z_{850}$  SBF data. Because of the greater efficiency of the F814W bandpass, the linear calibration defined by Equation (2) will allow accurate SBF distances to be measured with the ACS/WFC at greater distances than can be reached with the  $z_{850}$  band in the same amount of time. For instance, 4 orbits in  $I_{814}$  suffices for an SBF distance to the Coma cluster at 100 Mpc, whereas  $\sim 10$  orbits would be required in  $z_{850}$ .

The observed scatter in the calibration of  $\bar{M}_{814}$  as a function of  $(g_{475} - I_{814})$  is only 0.03 mag, significantly smaller than the expected  $\sim 0.06$  mag from intrinsic scatter in the method due to stellar population variations at a given color (Tonry et al. 1997; ACSFCS-V). This indicates that there is coherence between the intrinsic scatter in the  $z_{850}$  and  $I_{814}$  SBF relations, as expected from the similarity, and even partial overlap, of these passbands. Thus, stellar population effects cause the  $(\bar{m}_{814} - \bar{M}_{814})$  and  $(\bar{m}_{850} - \bar{M}_{850})$  distance moduli to scatter in the same direction, so that they are not fully independent. Direct comparison of the two sets of distances supports this conclusion, which helps to ensure a high degree of consistency between SBF distances measured in these two bands.

Comparison of our measurements with stellar population model predictions provides support for the empirically-based mean distance of 20 Mpc to the Fornax cluster. According to these models, and by analogy to the broader-baseline  $z_{850}$  SBF calibration, it is likely that the  $I_{814}$  SBF calibration will show curvature beyond the color limits of our sample. Therefore, the calibration should not be linearly extrapolated far beyond the range explored here. However, our sample was designed to have colors similar to those of the giant ellipticals targeted in more distant SBF studies; consequently, there should be little need for extrapolation. At least two different SBF studies in the F814W bandpass are ongoing and can benefit from our calibration. We have emphasized the need for good PSF templates in SBF measurements and the importance of investigating systematic variations due to the PSF. Our results indicate that when properly calibrated and controlled for systematics, the SBF method remains one of the most accurate ways of measuring extragalactic distances.

Support for this work was provided by NASA through grant number GO-10911 from the Space Telescope Science Institute, which is operated by AURA, Inc., under NASA contract NAS 5-26555. M.C. acknowledges support from COFIS ASI-INAF I/016/07/0 and PRIN-INAF 2008 (PI. M. Marconi). A.J. acknowledges support from BASAL CATA PFB-06, FONDAF CFA 15010003 and MIDEPLAN ICM Nucleus P07-021-F. This research made use of the NASA/IPAC Extragalactic Database (NED) which is operated by the Jet Propulsion Laboratory, California Institute of Technology, under contract with NASA.

*Facility*: HST (ACS/WFC)

## APPENDIX

### A. SBF SURVEY DISTANCE CORRECTIONS

Tonry et al. (2001; hereafter in this appendix, T01) published distances for 300 galaxies from the ground-based *I*-band SBF Survey of Galaxy Distances (Tonry et al. 1997). The median quoted uncertainty of 0.22 mag, just over 10% in distance, makes this the largest catalogue of nearby galaxy distances with this level of precision. It has proven a useful resource for numerous

extragalactic studies. However, following the publication of our combined sample of 134 galaxies with high-quality ACS  $z_{850}$ -band SBF distances (median error 0.075 mag) and the direct comparisons for 50 galaxies in common with T01, there has been some confusion over the possible need for correcting the T01 distances. As we have received more than a few queries on this issue, we address here in detail the question of the T01 distances, as well as those of Jensen et al. (2003; hereafter J03).

The ground-based SBF survey was conducted over numerous observing runs at multiple observatories with different types of detectors under variable seeing and photometric conditions during the course of a decade which saw great evolution in astronomical instrumentation and our own reduction software. It targeted galaxies ranging from the Local Group out to the fuzzy, condition-dependent limit of the ground-based SBF method. Although great effort was taken to homogenize the disparate data sets and produce the best possible set of final distances, the limitations of the data were already clear at the time; the authors recommended “further study of the degree of bias present in [the T01] data set” (see Sections 4 and 7 of T01).

A separate issue was the zero point. The calibration of the T01 distance catalogue was based on comparisons to six galaxies with *HST* Key Project (KP) Cepheid distances as tabulated by Ferrarese et al. (2000), which yielded an  $\bar{M}_I$  zero point of  $-1.74$  mag (Tonry et al. 2000). Blakeslee et al. (2002) found that when the calibration was rederived using the revised KP Cepheid distances from Freedman et al. (2001), the resulting zero-point shifted fainter to  $-1.68$  mag. If there were no distance-dependent biases, then this simple shift in zero point would mean that all the T01 distance moduli just needed to be revised downward by 0.06 mag. For instance, our ACSVCS papers applied this shift to the mean Virgo distance presented by T01, thus adopting 31.09 mag, or 16.5 Mpc, for Virgo. This was a reasonably “safe” assumption, given that the six galaxies used to tie together the SBF and Cepheid distances extended out to the Virgo cluster, and were generally targeted in above-average observing conditions. Note that some researchers have misinterpreted this 0.06 mag shift as resulting from a change in the adopted Hubble constant, but there is no explicit dependence on the Hubble constant, only a dependence on the zero point of the Cepheid distances.

In addition to rederiving the distance zero point based on the revised KP Cepheid distances, Blakeslee et al. (2002) found some evidence for distance bias in the lowest quality T01 data, in the sense that the relative distances tended to be underestimated for the lower quality data, as suspected by T01. This conclusion was based on comparisons with distances estimated from the fundamental plane and density field-corrected velocity measurements. Note that the absolute data quality generally decreases with distance, e.g., the errors increase with distance in T01, so this could potentially translate into a distance-dependent bias. Because of this combination of zero point and bias issues, Blakeslee et al. (2009) chose to compare the distances for the 50 galaxies in common between the T01 and ACS data sets without first applying any shifts to T01. This contrasted with our approach in Mei et al. (2007), where the comparison was made only for Virgo galaxies and the zero-point shift from Blakeslee et al. (2002) was applied; this difference may have been the cause of some subsequent confusion. Blakeslee et al. (2009) found the same mean Fornax distance modulus to within  $\pm 0.01$  mag as T01, without any shifting in zero point. However, the T01 Virgo distance modulus is then necessarily too high by 0.06 mag. As compared to the ACS studies, the data tabulated by T01 therefore give a smaller relative distance modulus of Fornax with respect to Virgo, although the uncertainties overlap. In light of these results, it becomes unclear whether or not a simple shift in the zero point of the T01 distance moduli is useful without a second-order correction that may depend on the distances of the galaxies under consideration. Given the 0.22 mag median error of the T01 distances, it could be argued that these effects are in the noise for any given galaxy. For galaxies within Virgo and Fornax, the tabulated ACS distances from Blakeslee et al. (2009) are much more accurate, and negligibly affected by the background variance corrections that were suggested to bias the ground-based data.

However, for some purposes, it may be desirable to have a general correction formula for the published T01 distances, including both the zero point and second-order bias corrections. Given our high-quality measurements for a sizable fraction of the T01 sample, we have attempted to derive one. We investigated possible correlations of the distance modulus difference  $\Delta_{T01} \equiv (m-M)_{ACS} - (m-M)_{T01}$ , where  $(m-M)_{ACS}$  comes from Blakeslee et al. (2009), with various quantities tabulated by T01 so that the correction is available for that full sample. In general, the correlations are weak, except between  $\Delta_{T01}$  and  $(m-M)_{T01}$ ; there is no significant correlation with  $(m-M)_{ACS}$ . This is easily understood if the ACSFCS-V distances are taken as the “true” values, or at least unbiased and homogeneous in quality; then the distance measurement error  $\Delta_{T01}$  will correlate strongly with the measured distance over any limited range in true distance. But this correlation, caused by measurement error, cannot be used to bias-correct the measured distances for the full sample. There is no correlation of  $\Delta_{T01}$  with the quoted measurement error, perhaps because of the relatively small range in the latter quantity and the multitude of effects that contribute to it.

It seemed more promising to investigate correlations with parameters that directly reflect the data quality. It is also necessary for the correction parameter to span reasonably well the same range in the current subsample as in the complete T01 catalogue. T01 supplied two measures of the quality of the data for each galaxy. One such parameter, called  $PD$ , was the normalized product of the width of the seeing disk in arcseconds and the expected distance based on the galaxy recessional velocity in units of 1000 km s $^{-1}$ , thus making it independent of any potential distance biases in the SBF distance measurement itself.  $PD$  is proportional to the linear size of the resolution element at the distance of the galaxy, and thus is smaller for better quality data. Another measure of data quality, called  $Q$  by T01 and here referred to as  $Q_{T01}$ , scaled logarithmically with the ratio of the signal-to-noise and  $PD$ ; thus it is larger for better quality data. Blakeslee et al. (2002) investigated bias as a function of  $PD$ ; we have found a slightly more significant trend as a function of  $Q_{T01}$ . Figure 7 shows  $\Delta_{T01}$  plotted against  $Q_{T01}$ . The fitted relation suggests that the T01 distance moduli can be bias-corrected according to

$$\begin{aligned} (m-M)_{T01, \text{cor}} &= (m-M)_{T01, \text{raw}} + 0.1 - 0.03 Q_{T01} \\ &= (m-M)_{T01, \text{raw}} - 0.03(Q_{T01} - 3.3). \end{aligned} \quad (\text{A1})$$

Thus, as published without any zero-point shifting, the poorest quality T01 distances with  $Q_{T01} \approx 1-2$  would be corrected by  $\sim +0.05$  mag, and the best quality ones with  $Q_{T01} \approx 7-8$  would be corrected by  $\sim -0.12$  mag. Given the range of  $Q_{T01}$  in Figure 7, we do not recommend applying corrections any larger than this. The six Cepheid calibrator galaxies have an average

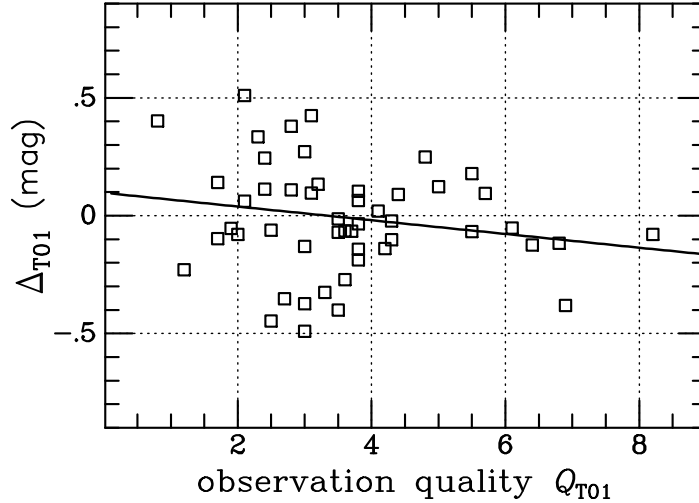


FIG. 7.— Difference between the Tonry et al. (2001) distance moduli and the ACSFCS-V distance moduli, defined such that  $\Delta_{T01} = (m-M)_{ACS} - (m-M)_{T01}$ , is plotted as a function of the Tonry et al. observation quality  $Q_{T01}$  for the 50 galaxies in common between the two samples. Note that the typical error on  $\Delta_{T01}$  is  $\sim 0.23$  mag, so the scatter is expected to be large. See Appendix for details.

$\langle Q_{T01} \rangle = 6.0$ , giving  $\langle \Delta_{T01} \rangle = -0.08$  mag, (or, omitting the Local Group galaxy M31:  $\langle Q_{T01} \rangle = 5.2$ ,  $\langle \Delta_{T01} \rangle = -0.06$  mag), very close to the expected shift from the Cepheid calibration, which is included within the correction formula. The significance of the fitted slope is only  $1.75\sigma$  based on these 50 galaxies, and the relative Fornax–Virgo distance modulus from the sample is unchanged, but if the trend persisted for the full T01 sample of 300 galaxies, the significance would reach  $4\sigma$ ; therefore studies relying on many T01 galaxy distances may benefit from applying a correction such as Equation (A1).

Finally, we address the J03 *HST*/NICMOS F160W SBF distances for 65 galaxies. These were tied to the KP Cepheid distances from Freedman et al. (2001), but without the espoused  $-0.2$  mag dex $^{-1}$  metallicity correction. The evidence for this correction was ambiguous at the time, and J03 found that the agreement with SBF predictions from stellar population models was better when the distance zero point was based on the Cepheid results without metallicity correction. Since then, there has been additional evidence to support a Cepheid metallicity dependence (Sakai et al. 2004; Macri et al. 2006; Scowcroft et al. 2009), and better understanding of the uncertainty in model predictions for near-IR SBF (Raimondo 2009; González-Lópezzira 2010; Lee et al. 2010). Given the high signal-to-noise and good resolution of the J03 NICMOS data, there is no reason to suspect a bias similar to that of T01. However, to bring them into agreement with other work requires putting them on the Cepheid scale that includes the metallicity correction. J03 derived their distance zero point by comparison to 47 T01 galaxies after shifting the distance moduli by  $-0.16$  mag, which comes from repeating the Tonry et al. (2000) calibration using the revised Cepheid distances without metallicity correction. As noted above, the change in the T01 moduli when calibrated on the revised Cepheid distances with metallicity correction is  $-0.06$  mag. This suggests a shift of  $+0.10$  mag to the Jensen et al. distance moduli, although there is some question about possible bias in the particular subsample of T01 that was used. J03 also measured SBF in nine KP Cepheid galaxies and tabulate the resulting  $\overline{M}_{160}$  values for the distances with and without metallicity correction; the mean difference is 0.08 mag, which is consistent with the shift in the T01 calibration caused by the metallicity correction. We therefore conclude that the J03 distance moduli should be increased uniformly by  $+0.1$  mag to bring them into consistency with the corrected T01 distances, our recent ACS  $z_{850}$  SBF measurements, and the present work.

#### B. ADDITIONAL ACSVCS DWARF GALAXY DISTANCES

Mei et al. (2007) published SBF measurements for 90 galaxies from the ACSVCS  $g_{475}$  and  $z_{850}$  imaging data, and Blakeslee et al. (2009) tabulated recalibrated distances for these along with the 43 ACSFCS galaxies and NGC 4697 in the Virgo Southern Extension. No SBF measurements were published for ten of the ACVCS galaxies, mainly owing to irregular morphologies. However, the problem for the galaxies VCC 1192 and VCC 1199 was different: they are both compact elliptical companions of the Virgo brightest cluster galaxy M49 (NGC 4472 or VCC 1226) and the strong background gradient from the giant galaxy’s halo caused the photometric measurements for these galaxies to be unreliable. Since the physical distances from M49 of these likely stripped (Ferrarese et al. 2006; Côté et al. 2010) companions are of interest, we have undertaken new measurements of these two galaxies. Although not directly related to the main content of this paper, these data are part of our larger *HST* SBF effort, and we present them here.

We constructed initial isophotal models of the light distributions of VCC1192 and VCC1199 in each filter. We then subtracted these models, masked the background sources, and interpolated two-dimensional cubic spline surfaces on a  $16 \times 16$  grid (each grid cell being  $\sim 270$  pix on a side) to make smooth fits of the background light distribution. Since these galaxies are so compact, and they had been removed by the initial models, they did not perceptibly affect the fits. After subtraction of the fitted surfaces, the backgrounds were extremely flat. We then constructed a new galaxy model for each and proceeded with the SBF and color measurements as usual, using the same code as in the present work. Table 3 presents our measurements for these galaxies in the same format as for the other ACSVCS galaxies in Table 2 of Blakeslee et al. (2009). This brings the total number of galaxies with measured  $z_{850}$  SBF distances to 136.

## REFERENCES

- Ajhar, E. A., Lauer, T. R., Tonry, J. L., Blakeslee, J. P., Dressler, A., Holtzman, J. A., & Postman, M. 1997, *AJ*, 114, 626
- Barber DeGraaff, R., Blakeslee, J. P., Meurer, G. R., & Putman, M. E. 2007, *ApJ*, 671, 1624
- Binggeli, B., Sandage, A., & Tammann, G.A., 1985, *AJ*, 90, 1681
- Biscardi, I., Raimondo, G., Cantiello, M., & Brocato, E. 2008, *ApJ*, 678, 168
- Blakeslee, J. P. 1999, *AJ*, 118, 1506
- Blakeslee, J. P., Anderson, K. R., Meurer, G. R., Benítez, N., & Magee, D. 2003, *Astronomical Data Analysis Software and Systems XII*, 295, 257
- Blakeslee, J. P., Lucey, J. R., Tonry, J. L., Hudson, M. J., Narayanan, V. K., & Barris, B. J. 2002, *MNRAS*, 330, 443
- Blakeslee, J. P., Tonry, J. L., & Metzger, M. R. 1997, *AJ*, 114, 482
- Blakeslee, J. P., Vazdekis, A., & Ajhar, E. A. 2001, *MNRAS*, 320, 193
- Blakeslee, J. P., et al. 2006, *ApJ*, 644, 30
- Blakeslee, J. P., et al. 2009, *ApJ*, 694, 556 (ACSFC5-V)
- Bohlin, R. C. 2007, *Instrument Science Report ACS-2007-006* (Baltimore: STScI)
- Buzzoni, A. 1993, *A&A*, 275, 433
- Cantiello, M., Blakeslee, J. P., Raimondo, G., Mei, S., Brocato, E., & Capaccioli, M. 2005, *ApJ*, 634, 239
- Cantiello, M., Blakeslee, J., Raimondo, G., Brocato, E., & Capaccioli, M. 2007a, *ApJ*, 668, 130
- Cantiello, M., Raimondo, G., Blakeslee, J. P., Brocato, E., & Capaccioli, M. 2007b, *ApJ*, 662, 940
- Cantiello, M., Raimondo, G., Brocato, E., & Capaccioli, M. 2003, *AJ*, 125, 2783
- Côté, P., et al. 2004, *ApJS*, 153, 223
- Côté, P., et al. 2010, *ApJ*, submitted
- Dunn, L. P., & Jerjen, H. 2006, *AJ*, 132, 1384
- Ferguson, H.C. 1989, *AJ*, 98, 367
- Ferrarese, L., et al. 2000, *ApJ*, 529, 745
- Ferrarese, L., et al. 2006, *ApJS*, 164, 334
- Freedman, W. L., et al. 2001, *ApJ*, 553, 47
- Freedman, W. L., & Madore, B. F. 2010, *arXiv:1004.1856*
- Fruchter, A. S. & Hook, R. N. 2002, *PASP*, 114, 144
- González-Lópezlira, R. A., Bruzual-A., G., Charlot, S., Ballesteros-Paredes, J., & Loinard, L. 2010, *MNRAS*, 403, 1213
- Hubble, E. 1929, *Proceedings of the National Academy of Science*, 15, 168
- Hubble, E. P. 1926, *ApJ*, 64, 321
- Jensen, J. B., Tonry, J. L., Barris, B. J., Thompson, R. I., Liu, M. C., Rieke, M. J., Ajhar, E. A., & Blakeslee, J. P. 2003, *ApJ*, 583, 712 (J03)
- Jensen, J. B., Tonry, J. L., & Luppino, G. A. 1998, *ApJ*, 505, 111
- Jensen, J. B., Tonry, J. L., Thompson, R. I., Ajhar, E. A., Lauer, T. R., Rieke, M. J., Postman, M., & Liu, M. C. 2001, *ApJ*, 550, 503
- Jordán, A., Blakeslee, J. P., Côté, P., Ferrarese, L., Infante, L., Mei, S., Merritt, D., Peng, E. W., Tonry, J. L., West, M. J. 2007, *ApJS*, 169, 213
- Jordán, A., Blakeslee, J. P., Peng, E. W., Mei, S., Côté, P., Ferrarese, L., Tonry, J. L., Merritt, D., Milosavljević, M., West, M. J. 2004, *ApJS*, 154, 509
- Krist, J. 2003, *STScI Instrument Status Report ACS2003-06*
- Leavitt, H. S. 1908, *Annals of Harvard College Observatory*, 60, 87
- Lee, H.-c., Worthey, G., & Blakeslee, J. P. 2010, *ApJ*, 710, 421
- Liu, M. C., Graham, J. R., & Charlot, S. 2002, *ApJ*, 564, 216
- Lorenz, H., Bohm, P., Capaccioli, M., Richter, G. M., & Longo, G. 1993, *A&A*, 277, L15
- Macri, L. M., Stanek, K. Z., Bersier, D., Greenhill, L. J., & Reid, M. J. 2006, *ApJ*, 652, 1133
- Marín-Franch, A., & Aparicio, A. 2006, *A&A*, 450, 979
- Mei, S., Blakeslee, J.P., Tonry, J.L., Jordán, A., Peng, E.W., Côté, P., Ferrarese, L., Merritt, D., Milosavljević, M., & West, M.J. 2005a, *ApJS*, 156, 113
- Mei, S., Blakeslee, J.P., Tonry, J.L., Jordán, A., Peng, E.W., Côté, P., Ferrarese, L., West, M.J., Merritt, D., & Milosavljević, M. 2005b, *ApJ*, 625, 121
- Mei, S., Blakeslee, J. P., Côté, P., Tonry, J. L., West, M. J., Ferrarese, L., Jordán, A., Peng, E. W., Anthony, A., & Merritt, D. 2007, *ApJ*, 655, 144
- Mei, S., Quinn, P. J., & Silva, D. R. 2001, *A&A*, 371, 779
- Mieske, S., Hilker, M., & Infante, L. 2003, *A&A*, 403, 43
- Neilsen, E. H., Jr., & Tsvetanov, Z. I. 2000, *ApJ*, 536, 255
- Pahre, M. A., et al. 1999, *ApJ*, 515, 79
- Raimondo, G. 2009, *ApJ*, 700, 1247
- Raimondo, G., Brocato, E., Cantiello, M., & Capaccioli, M. 2005, *AJ*, 130, 2625
- Sakai, S., Ferrarese, L., Kennicutt, R. C., Jr., & Saha, A. 2004, *ApJ*, 608, 42
- Schlegel, D.J., Finkbeiner, D.P., & Davis, M. 1998, *ApJ*, 500, 525
- Scowcroft, V., Bersier, D., Mould, J. R., & Wood, P. R. 2009, *MNRAS*, 396, 1287
- Sirianni, M., et al. 2005, *PASP*, 117, 1049
- Tonry, J.L. 1991, *ApJ*, 373, L1
- Tonry, J.L., Ajhar, E.A., & Luppino, G.A. 1990, *AJ*, 100, 1416
- Tonry, J. L., Blakeslee, J. P., Ajhar, E. A., & Dressler, A., 1997, *ApJ*, 475, 399
- Tonry, J. L., Blakeslee, J. P., Ajhar, E. A., & Dressler, A., 2000, *ApJ*, 530, 625
- Tonry, J.L., Dressler, A., Blakeslee, J.P., Ajhar, E.A., Fletcher, A.B., Luppino, G.A., Metzger, M.R., & Moore, C.B. 2001, *ApJ*, 546, 681 (T01)
- Tonry, J.L., & Schneider, D.P. 1988, *AJ*, 96, 807
- Worthey, G. 1993, *ApJ*, 409, 530

TABLE 1  
 GALAXY DATA

Galaxy (1)	$B_T$ (2)	Morph (3)	$v_h$ (4)	Other (5)	$T_{F475}$ (6)	$T_{F814}$ (7)	$(m-M)_{850}$ (8)	Program (9)
NGC 1316	9.4	S0 pec	1760	FCC 21	760	4680	$31.607 \pm 0.065$	10217,9409
NGC 1344	11.3	E5	1169	NGC 1340	760	960	$31.603 \pm 0.068$	10217,9399
NGC 1374	11.9	E0	1294	FCC 147	680	1224	$31.459 \pm 0.070$	10911
NGC 1375	13.6	S0	740	FCC 148	680	1224	$31.499 \pm 0.072$	10911
NGC 1380	11.3	S0/a	1877	FCC 167	680	1224	$31.632 \pm 0.075$	10911
NGC 1399	10.6	E1	1425	FCC 213	680	1224	$31.596 \pm 0.091$	10911
NGC 1404	10.9	E2	1947	FCC 219	680	1224	$31.526 \pm 0.072$	10911
NGC 1427	11.8	E4	1388	FCC 276	680	1224	$31.459 \pm 0.068$	10911
IC 2006	12.2	E2	1382	ESO 359-07	680	1224	$31.525 \pm 0.086$	10911

NOTE. — Columns list: (1) galaxy name; (2) total  $B$  magnitude from the FCC (Ferguson 1989) or NED; (3) morphological type from the FCC or NED; (4) heliocentric velocity from NED ( $\text{km s}^{-1}$ ) (5) alternative galaxy designation; (6) *HST*/*ACS* exposure time for the F475W bandpass (sec); (7) *HST*/*ACS* exposure time for the F814W bandpass (sec); (8) distance modulus and uncertainty from  $z_{850}$ -band SBF (ACSFCS-V); (9) *HST* program IDs for the observations used in this study.

 TABLE 2  
 GALAXY COLOR AND SBF MEASUREMENTS

Galaxy (1)	$(g-I)$ (2)	$\bar{m}_{814}$ (3)	$(m-M)_{814}$ (4)	$d_{814}$ (Mpc) (5)
NGC 1316	$1.177 \pm 0.011$	$30.428 \pm 0.020$	$31.638 \pm 0.066$	$21.3 \pm 0.7$
NGC 1344	$1.131 \pm 0.015$	$30.315 \pm 0.039$	$31.609 \pm 0.076$	$21.0 \pm 0.7$
NGC 1374	$1.193 \pm 0.022$	$30.286 \pm 0.015$	$31.467 \pm 0.074$	$19.7 \pm 0.7$
NGC 1375	$1.065 \pm 0.009$	$30.116 \pm 0.037$	$31.530 \pm 0.072$	$20.2 \pm 0.7$
NGC 1380	$1.232 \pm 0.011$	$30.460 \pm 0.016$	$31.570 \pm 0.065$	$20.6 \pm 0.6$
NGC 1399	$1.315 \pm 0.017$	$30.662 \pm 0.022$	$31.620 \pm 0.071$	$21.1 \pm 0.7$
NGC 1404	$1.277 \pm 0.014$	$30.516 \pm 0.018$	$31.544 \pm 0.068$	$20.4 \pm 0.6$
NGC 1427	$1.171 \pm 0.019$	$30.213 \pm 0.017$	$31.434 \pm 0.072$	$19.4 \pm 0.6$
IC 2006	$1.234 \pm 0.016$	$30.430 \pm 0.035$	$31.536 \pm 0.075$	$20.3 \pm 0.7$

NOTE. — Columns list: (1) galaxy name; (2) mean galaxy  $(g_{475}-I_{814})$  color; (3) mean SBF magnitude  $\bar{m}_{814}$ ; (4) distance modulus derived from the linear  $I_{814}$  SBF calibration presented here; (5) the distance in Mpc. The distance errors include contributions from SBF and color measurement errors, as well as the estimated intrinsic (“cosmic”) scatter in the method.

 TABLE 3  
 DISTANCES FOR ADDITIONAL ACS VIRGO CLUSTER SURVEY GALAXIES

Galaxy (1)	$(g-z)$ (2)	$\bar{m}_z$ (3)	$(m-M)$ (4)	$d$ (5)	$B_T$ (6)	Name (7)
VCC1192	$1.443 \pm 0.009$	$29.305 \pm 0.065$	$31.078 \pm 0.091$	$16.4 \pm 0.7$	15.0	NGC4467
VCC1199	$1.469 \pm 0.030$	$29.345 \pm 0.169$	$31.055 \pm 0.196$	$16.3 \pm 1.5$	15.5	...

NOTE. — Columns list: (1) VCC designation (Binggeli et al. 1985); (2) mean  $(g_{475}-z_{850})$  color of the analyzed region; (3) mean F850LP SBF magnitude  $\bar{m}_z$ ; (4) distance modulus derived from Equation [6] of ACSFCS-V; (5) distance in Mpc; (6) total  $B$  magnitude from the VCC or NED; (7) common galaxy name.